JPE 7-2-2

Advanced Control of a PWM Converter with a Variable-Speed Induction Generator

Tarek Ahmed†, Katsumi Nishida**, Mutsuo Nakaoka* and Toshihiko Tanaka*

†*The Graduate School of Science and Engineering, Yamaguchi University, Yamaguchi, Japan
**Ube National College of Technology, Ube city, Yamaguchi, Japan

ABSTRACT

This paper describes simple control structures for a vector controlled stand-alone induction generator (IG) for use under variable speeds. Different control principles, indirect vector control and deadbeat current control, are developed for a voltage source PWM converter and the three-phase variable speed squirrel-cage IG to regulate DC-link and generator voltages with a newly designed phase locked loop circuit. The required reactive power for the variable speed IG is supplied by means of a PWM converter and a capacitor bank to buildup the voltage of the IG without the need for a battery, to reduce the rating of the PWM converter while using only three sensors and to eliminate the harmonics generated by the PWM converter. These proposed schemes can be used efficiently for variable speed wind energy conversion systems. The measurements of the IG systems at various speeds and loads are given and show that these systems are capable of good AC and DC voltage regulation.

Keywords: Induction Generator, Vector and Deadbeat Current Control, AC and DC Power Applications, PWM Converter

1. Introduction

The general consciousness of finite and limited sources of energy on earth and international disputes over the environment, global safety, and the quality of life have created an opportunity for new, more efficient, less polluting wind and hydro power plants which use advanced technologies of control, robustness, and modularity. The induction generator (IG), with its lower maintenance demands and simplified controls, appears to be a good solution for such applications[1]. Due to its simplicity, robustness, and small size per generated kW, the induction generator is favored for small hydro and wind power plants. It has great economic appeal. Standing alone, its maximum power does not go much beyond 15 kW[3-4]. So, we need to think in terms of a spectrum of power supplies from small (few Watts) to large (100 kW or more). However, the major drawbacks of induction generators are reactive power consumption and poor voltage regulation at varying speeds, but the development of static power converters has facilitated the control of the output voltage of IGs[5-9].

An induction-machine-based stand-alone power generation scheme with a diode bridge rectifier and a

Manuscript received December 12, 2005; revised Feb. 7, 2007
†Corresponding Author: TarekAhmed@ieee.org
Tel: +81-836-85-9472, Fax: +81-836-85-9401, Yamaguchi Univ.
*Yamaguchi Univ.
**Ube National College of Technology

PWM converter that uses the rotor field orientation has been proposed to control the output voltage of the diode bridge rectifier[7]. However, there is a serious voltage harmonics problem with this proposed scheme. Moreover, the magnetization curve has not been included for improving accuracy in calculating the rotor flux position. Based on the instantaneous reactive power theory, using a capacitor bank and an inverter simultaneously without any mechanical position sensor in the induction machine rotor has been proposed [8]. There are many voltage and current sensors that have been used to achieve the desired result of the proposed strategy, but they regulate AC voltage poorly, especially at low speeds.

In this paper aspects related to voltage regulation using sensorless vector control strategies for a forced-commutated voltage source PWM converter connected to a stand-alone induction generator in wind, mini/micro-hydro energy application are investigated. Different control principles have been used on the voltage source converter and three-phase squirrel-cage induction generator. A hybrid excitation unit, consisting of a capacitor bank and a PWM converter, is used for the IG loaded with three-phase loads and DC loads. This is a more reliable and simpler method of IG voltage control; it can start and generate its output voltage and reduce the rating of the PWM converter. The capacitor bank and converter can supply the required reactive power to regulate both the IG output and DC link voltages.

2. Indirect Vector Controlled IG with PWM Converter and Capacitor Bank

The IG in Fig.1 is controlled in a synchronously rotating *d-q* axis frame, with the *d*-axis oriented along the rotor-flux vector position. In this approach, a decoupled control between the reactive and active currents is obtained. The stator reactive and active currents are varied to control the AC output voltage of the IG and the DC-link voltage under variable speeds and different load types.

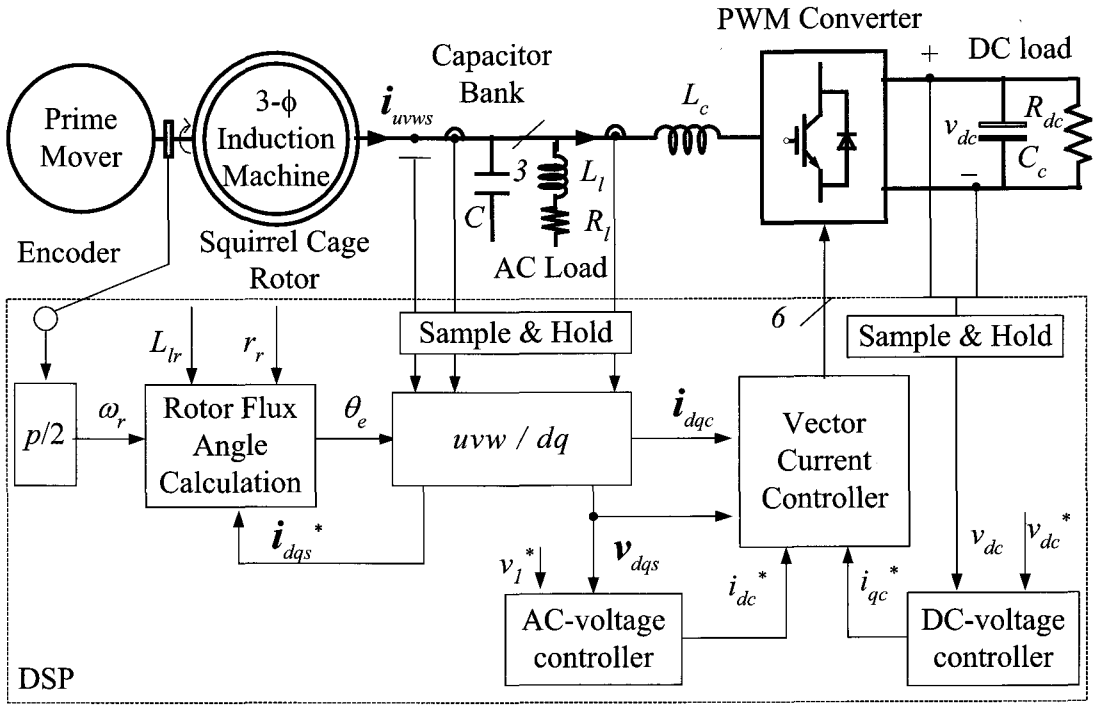

Fig. 1 Induction generator for small-scale AC and DC power applications

Under the rotor field-oriented control, the rotor-flux vector position θ_e is calculated from,

$$\theta_e = \int \left(\frac{L_m i_{qs}}{\tau_r \lambda_{dr}} + \omega_r \right) dt \tag{1}$$

where, the magnitude of the rotor flux in steady-state is, $\lambda_{dr} = L_m i_{ms} = L_m i_{ds}$ and τ_r (L_r / r_r) is the rotor time constant of the induction machine and the equivalent-circuit parameters, L_{ls}=3.65 mH, L_{lr}=3.65 mH, r_s=0.63 Ω, and r_r=0.63 Ω, are obtained by the experimental measurements on a laboratory 2.2 kW, 220 V, 8.0 A, 60 Hz, 4-poles, squirrel-cage induction machine. Since the stator of the IG is connected to an isolated load, the stator magnetizing current i_{ms} cannot be considered constant. The relationship between the magnetizing inductance L_m and the magnetizing phase current i_m ($i_m = i_{ms} / \sqrt{2}$) is obtained experimentally and expressed as,

$$L_m = \frac{1}{120\pi} \left\{ \begin{matrix} -0.1175\, i_m^5 + 1.918\, i_m^4 - 11.074\, i_m^3 \\ +25.387\, i_m^2 - 19.662\, i_m + 53.365 \end{matrix} \right\} \tag{2}$$

The accuracy of the rotor flux angle is critical to the rotor vector control where the calculation of currents such as the *d-q* axis currents of the IG, i_{ds} and i_{qs} in the synchronous frame is determined by the electrical rotor flux angle θ_e. Therefore, this vector control method relies on knowledge of the magnetizing inductance L_m, the real values of which may be changing as operating conditions change. In simulation, the block diagram of the rotor-flux vector position θ_e is depicted in Fig.2 while the integral in (1) is solved in the experiment by using a digital filter, with a cutoff frequency of 0.5 Hz to eliminate DC offset.

2.1 Design of IG Output Voltage Loop

The block diagram of the simplified model of the IG output voltage control loop is shown in Fig.3. Assuming the inner loops of the *d-q* axis currents are ideal and v_1^* ($v_1^* = \left(\sqrt{3/2}\right)\sqrt{v_{qs}^2 + v_{ds}^2} \cong \left(\sqrt{3/2}\right) v_{qs}$). The transfer function of the *q*-axis voltage to the *d*-axis IG reference current is,

$$\frac{v_{qs}(s)}{i_{ds}^*(s)} = \frac{\omega L_m}{(1+\tau_r s)} \tag{3}$$

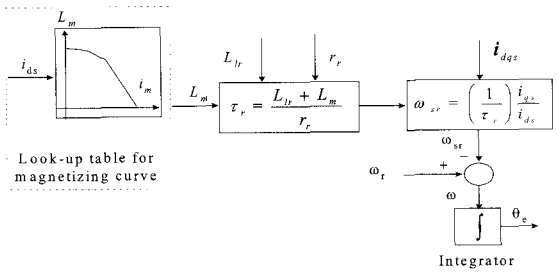

Fig. 2 Block diagram for rotor flux angle calculation

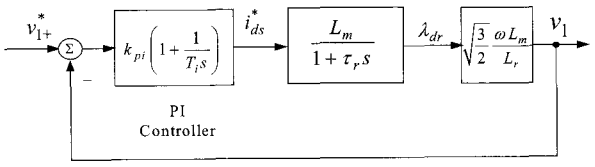

Fig. 3 IG-output voltage control loop

Observing Fig.3, the whole transfer function is written as,

$$\frac{v_1(s)}{v_1^*(s)} = \sqrt{\frac{3}{2}} \frac{\omega L_m^2 k_{ii}}{\tau_r L_r} \frac{(T_i s + 1)}{\left(s^2 + 2\zeta_i \omega_{ni} s + \omega_{ni}^2\right)} \tag{4}$$

The parameters k_{pi}, T_i of the PI controller are given by,

$$k_{pi} = \sqrt{\frac{2}{3}} \frac{L_r}{\omega L_m^2} \left(2\xi_i \tau_r \omega_{ni} - 1\right) \quad \text{and}$$

$$T_i = \frac{k_{pi}}{k_{ii}} = \frac{\left(2\xi_i \tau_r \omega_{ni} - 1\right)}{\tau_r \omega_{ni}^2} \tag{5}$$

Using the parameters, τ_r =0.113 s and L_m = 0.0661 H, at the full-load and rated speed ω = 377 rad.s^{-1} with damping ratio $\xi = \sqrt{2}/2$, the parameters of the PI controller are, k_{Pi} =0.0611 AV^{-1}, k_{ii}= 1.26 A(Vs)$^{-1}$and T_i = 0.0485 *s* to give the closed-loop natural frequency ω_{ni} = 20 rad.s^{-1}.

3. Sensorless Vector Controlled IG with PWM Converter and Capacitor Bank

Fig.4 shows the schematic configuration of the advanced deadbeat current strategy for the stand-alone IG

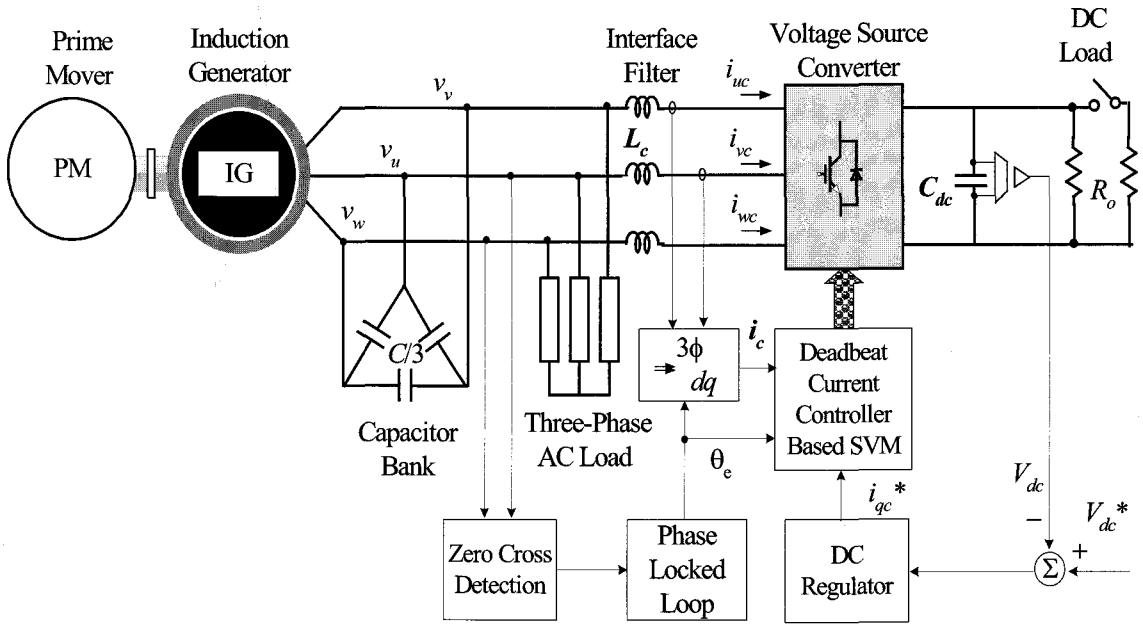

Fig. 4 Schematic diagram of sensorless control of IG with PWM converter equipped with deadbeat controller

excited by using both the capacitor bank and the PWM converter simultaneously. A designed phase locked loop circuit (PLL) and only three sensors are necessary for detecting the DC-bus voltage and the input-side currents of the PWM converter. This control strategy enables us to reduce the PWM converter rating and estimate the IG output voltage while obtaining good voltage regulation under variable speeds and loads. Moreover, the proposed system does not need any mechanical position sensor. A particular rotating reference frame is useful for analyzing the IG system by choosing the rotating q-axis to be the angle of the stator voltage, v_s of the IG. The quadrature voltage component of the stator voltage v_{qs} always coincides with the rotating q-axis frame. In fact, this choice offers a lot of advantages for simplifying the control and analysis of the IG system. To align the stator voltage on the q-axis with the direct voltage component of the stator voltage v_{ds} equal to zero, the zero cross point of the line-to-line voltage v_{vw} is required as the reference signal for the designed phase locked loop circuit (PLL) to determine the electrical angle of the IG stator voltage as indicated in Fig.4.

3.1 Steady-State Equivalent Circuit of IG System with Deadbeat Current Controller

A model of the IG system using the stator vector reference frame can be obtained from the well known dynamic model

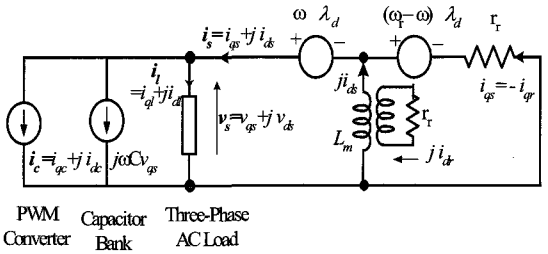

Fig. 5 Equivalent circuit of simplified IG system in stator voltage vector reference frame

of the induction machine by substituting v_{ds} = 0 and neglecting the induction machine leakage inductances and stator resistances[5-7]. The steady-state equivalent circuit of the simplified IG system is depicted in Fig.5. From the simplified steady-state model of the stand-alone IG system depicted in Fig.5, v_{ds}=0, λ_{qs}=λ_{qr} =0, i_{dr} =0, i_{qs} =– i_{qr} and λ_{ds} = L_m i_m = L_m i_{ds}. Moreover, the quadrature stator voltage; v_{qs} depends on the stator reactive current; i_{ds} as stated in the following equation:

$$v_{qs} = \omega \lambda_d = \omega L_m i_{ds} \tag{6}$$

where, ω ($\omega = \omega_r - i_{qs}/(\tau_r i_{ds})$) is the electrical angular frequency and τ_r ($\tau_r = L_m/r_r$) is the rotor time constant.

3.2 Design of Capacitor Bank

From Fig.5, the stator reactive-current of the IG needed to generate the rated voltage under the no-load and the rated speed conditions is given by:

$$i_{ds} = \omega\ C\ v_{qs} \tag{7}$$

By substituting the stator voltage v_{qs} of (7) into (6), the capacitance of the capacitor bank is defined as follows,

$$C = \frac{1}{\omega^2 L_m} \tag{8}$$

From (8) and (2), the minimum capacitance; C_{min} required for building-up the stand-alone IG voltage at the rated speed n =1800 rpm, is estimated with $L_m = L_{unsm}$ = 53.365/(120π) H where L_{unsm} is the unsaturated magnetizing inductance. Therefore, the minimum required excitation capacitance for the IG under the no-load and the rated speed conditions is $C_{min} \cong 50\ \mu$ F.

3.3 Current Control of IG and PWM Converter

From Fig.5, the stator reactive current i_{ds} of the IG, defined as the sum of the uncontrolled capacitor bank current, the three-phase load reactive current i_{dl} and the converter reactive current i_{dc} is given by:

$$i_{ds} = \omega\ C\ v_{qs} + i_{dl} + i_{dc} \tag{9}$$

While the stator active current i_{qs} of the IG, obtained by adding the three-phase load active current i_{ql} to the converter active current i_{qc}, is written as follows:

$$i_{qs} = i_{ql} + i_{qc} \tag{10}$$

Therefore, the AC voltage regulation of the IG can be implemented by a control loop that drives the converter reactive current i_{dc} ; the DC bus voltage regulation of the IG scheme can also be implemented by a control loop that drives the converter active current i_{qc}.

Fig.6 shows the block diagram of the proposed deadbeat current controller with two PI regulators: the AC stator voltage regulator and the DC link voltage regulator. The input of the DC link voltage regulator is the difference between the DC link voltage reference and the measured value, while its output has been defined as the active current reference i_{qc}^* of the PWM converter. Also, the input of the AC stator voltage regulator is the difference between the stator voltage reference and the estimated stator voltage. Its output has been defined as the stator reactive current reference i_{dc}^*. This reference must be limited to avoid the induction machine saturation. The PI parameters for DC regulation are set at K_P(Proportional Gain)=0.15 [A/V] and K_I(Integral Gain)= 6.0 [A/(Vs)] respectively. The reference current space vector of the PWM converter is then defined by:

$$\boldsymbol{i}_c^* = i_{qc}^* + j\, i_{dc}^* \tag{11}$$

3.4 Deadbeat Current Control for Voltage Source Converter

Fig.7 represents the power circuit of the three-phase voltage-source converter using IGBT power modules. The voltage balance across the AC side interface filters in the stationary α-β reference frame; $\omega = 0$ is written by;

$$\boldsymbol{v}_s = \left(R_c + \frac{d}{dt} L_c \right) \boldsymbol{i}_c + \boldsymbol{v}_c \tag{12}$$

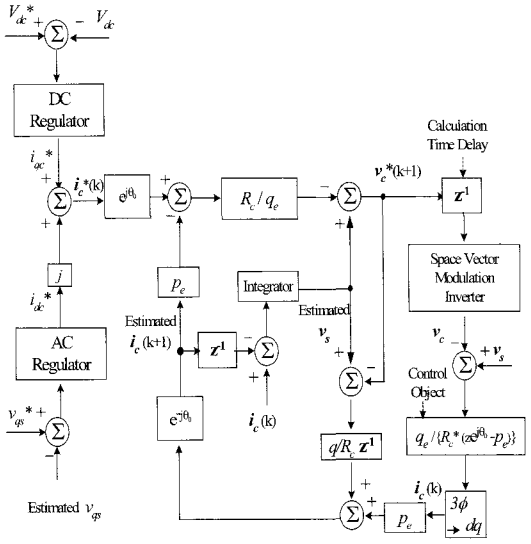

Fig. 6 Proposed deadbeat control scheme for AC and DC voltage regulation of IG with PWM converter

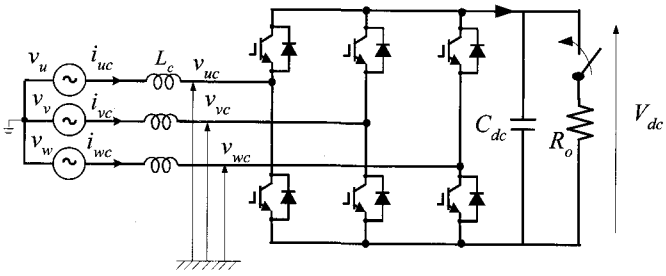

Fig. 7 Power circuit of voltage-source converter using IGBT modules

where, R_c and L_c are the resistance and inductance of the AC side filter of the PWM converter. $\boldsymbol{v}_s$ is the IG's output voltage vector, $\boldsymbol{i}_c$ is the current vector of the PWM converter and $\boldsymbol{v}_c$ is the output voltage vector of the PWM converter. During a sampling time T_s, $\boldsymbol{v}_s$ and $\boldsymbol{v}_c$ in (12) are assumed to be constant. In this case, the above equation can be discretized and arranged as follows:

$$\boldsymbol{i}_c(k+1) = p_e \boldsymbol{i}_c(k) + \frac{q_e}{R_c}\{\boldsymbol{v}_s(k) - \boldsymbol{v}_c(k)\} \quad (13)$$

In order to carry out the deadbeat control strategy easily, it is necessary to implement the control algorithm on a *d-q* synchronous rotating frame. It is important to estimate the control variable of one sampling period ahead of the current space vector $\boldsymbol{i}_c$ (k+1) of the PWM converter to control it with high accuracy to cancel the calculation time delay in the DSP. The prediction of $\boldsymbol{i}_c$ (k+1) can easily be made by using the following equation in the *d-q* synchronous rotating frame:

$$\overline{\boldsymbol{i}_c(k+1)} = \left\{ p_e\, \boldsymbol{i}_c(k) + \frac{q_e}{R_c}\left[\overline{\boldsymbol{v}_s(k)} - \boldsymbol{v}_c(k)\right] \right\} e^{-j\theta_0} \quad (14)$$

where, $p_e = e^{-R_c T_s / L_c}$, $q_e = 1 - p_e$ and $\theta_0 = \omega T_s$.

The output voltage of the PWM converter can be calculated at a sampling point (k+1) as follows:

$$\boldsymbol{v}_c^*(k+1) = \overline{\boldsymbol{v}_s(k)} - \frac{R_c}{q_e}\left\{ e^{j\theta_0}\, \boldsymbol{i}_c^*(k) - p_e\, \overline{\boldsymbol{i}_c(k+1)} \right\} \quad (15)$$

In Fig.6, the stator voltage $\boldsymbol{v}_s$ [$\boldsymbol{v}_s = v_{qs} + jv_{ds}$, where $v_{ds} = 0$] of the IG can only be estimated by using an integrator, because $\boldsymbol{v}_s$ is equal to the disturbance in the current control system of the PWM converter. Therefore, the stator voltage space vector $\boldsymbol{v}_s$ of the IG is calculated using the following equation:

$$\overline{\boldsymbol{v}_s(z)} = K_I \frac{z}{z-1}\left\{ \boldsymbol{i}_c(z) - \overline{\boldsymbol{i}_c(z)} \right\} \quad (16)$$

where, K_I is the integrating gain which is set at 1.25 [V/A].

3.5 Experimental Setup of IG and PWM Converter

In Fig.8, the implementation system for the AC and DC voltage regulation of the stand-alone IG and the PWM converter is carried out. All calculations are accomplished digitally based on the deadbeat current control algorithm for controlling the AC-side currents of the PWM converter while determining the AC-side space voltage vector of the PWM converter. The control circuit consists of A/D converters, a DSP, a PLL circuit, a PWM board, and a zero crossing detector circuit. Among these, three A/D converters (AD7572A) are used to convert analog signals to digital ones. A/D converters are used to sample the PWM converter AC side currents i_{uc}, i_{vc} and the voltage V_{dc} across the DC bus capacitor of the PWM converter. AD7572A is a complete analog to digital converter that offers high speed performance (a conversion time of 3 μs) combined with low CMOS power levels. The 16-bit fixed decimal point 40-MIPS DSP, TMS320C542, which has separate program and data spaces, allows simultaneous access to program instructions and data and provides a high degree of parallelism. A fixed point DSP is chosen over a floating point DSP to reduce the overall IG system cost.

The line voltage signal of the IG output voltage is detected through a potential transformer (PT) to detect its zero crossing point. Then, the zero-crossing signal is sent to the interruption terminal of the DSP (Int-0) and the phase comparator as the reference in the PLL circuit. However, this zero-crossing signal is used for determining the direction of *q*-axis on the α-β stationary coordinate frame in synchronization with the IG line voltage. In Fig.9, the newly designed PLL circuit consists of a phase

comparator, loop filter, voltage controlled oscillator (VCO) and synchronous counters. From Fig.10, it has been recognized that the appropriate design of the loop pass filter plays an important role in achieving good performance of the PLL circuit and the required stability of the IG system. The ripple components in Channel 4 of Fig.10 are observed. These ripple components can be reduced by setting both time constants R_1C_1 and R_3C_3 at higher values. However, increasing these time constants results in poor responsiveness of the IG system.

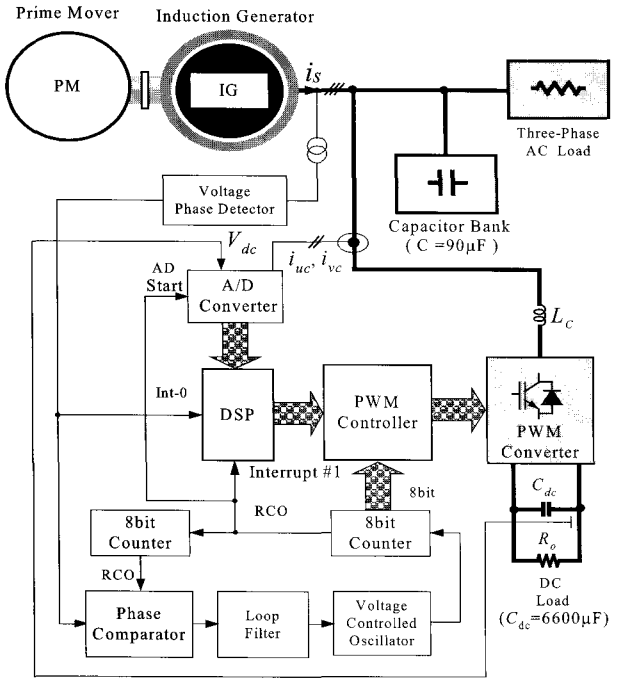

Fig. 8 DSP based experimental setup for the proposed IG and PWM converter

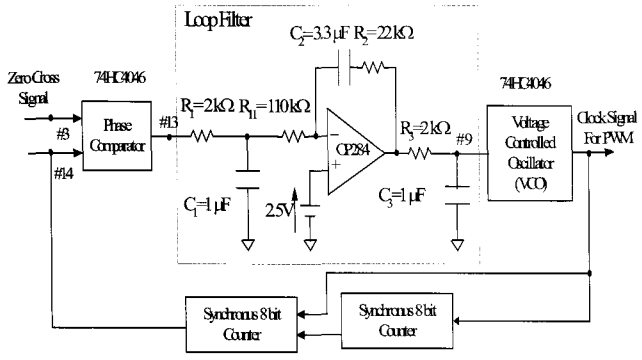

Fig. 9 Phase locked loop circuit with newly designed loop filter

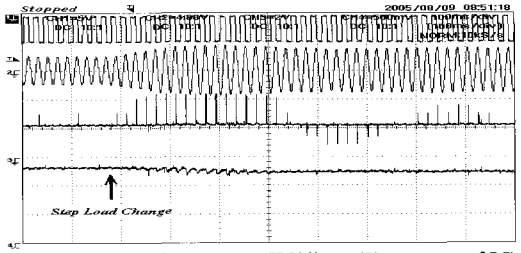

(1) MSB of upper 8 bit counter: 5V/div (2) current of IG stator: 10A/div (3)loop filter input(#13) : 2V/div (4) loop filter output(#9) : 0.5V/div

Fig. 10 Measured transient response of the proposed PLL circuit

4. Voltage Regulation with DC Load

Several tests have been carried out to study the performance under both transient and steady-state conditions for DC load only. Figs.11 and 12 show the measured waveforms of the AC-side current of the PWM converter, the IG current and the line-to-line voltage and DC link voltage at a step change in the DC load power from 16% to 50% of the full-load at n = 1760 rpm and n = 1330rpm, respectively. These waveforms demonstrate the capability of the converter to control the DC link voltage and the IG output voltage by controlling the reactive power to the IG, or the reactive power from the fixed capacitor. At the same time, the reactive and active currents responses of the PWM converter to the step change in DC load power are also depicted. The reactive current demand depends mainly on the speed. This proposed control system provides good voltage regulation of the DC load and IG voltages for speed 1760 rpm and for low speeds less than 1400 rpm where the IG could be advantageous in wind power applications.

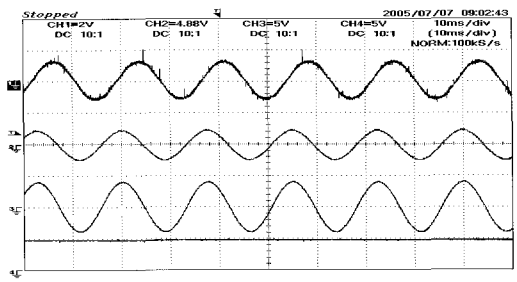

(1) Converter AC-side current -5A/div (2) IG current -5A/div (3) IG voltage -250V/div (4) DC link voltage -250V/div

(a) before step change, 57.3 Hz

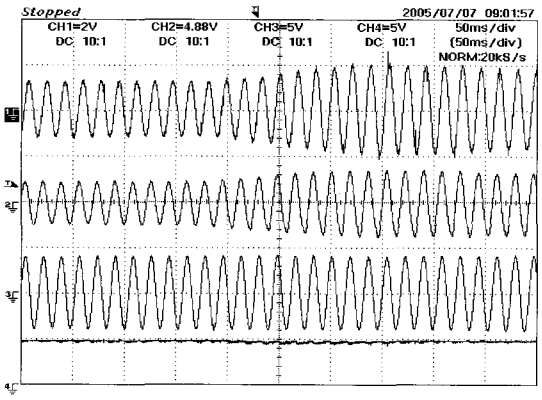

(1) Converter AC-side current -5A/div (2) IG current -5A/div
(3) IG voltage -250V/div (4) DC link voltage -250V/div

(b) in transient, 57.3 Hz-56.7 Hz

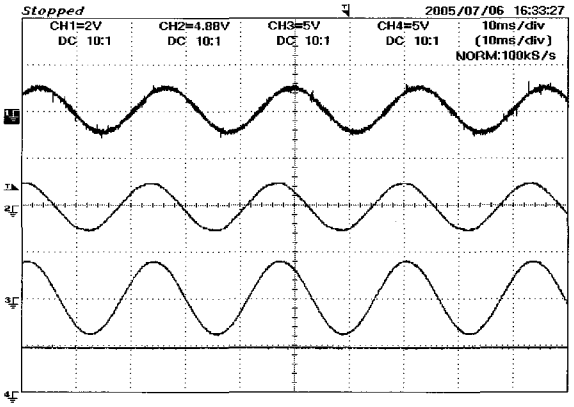

(1) Converter AC-side current -5A/div (2) IG CURRENT -5A/div
(3) IG voltage -250V/div (4) DC LINK VOLTAGE -250V/div

(a) before step change 43.1Hz

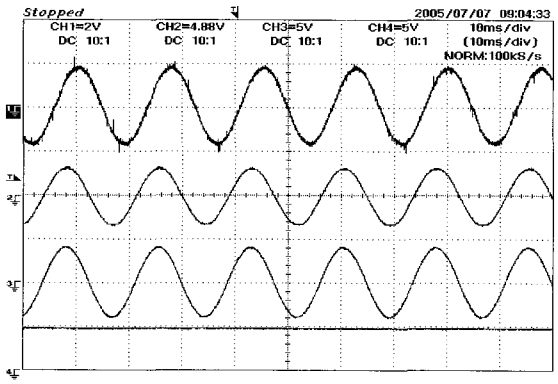

(1) Converter AC-side current -5A/div (2) IG current -5A/div
(3) IG voltage -250V/div (4) DC link voltage -250V/div

(c) after step change, 56.7 Hz

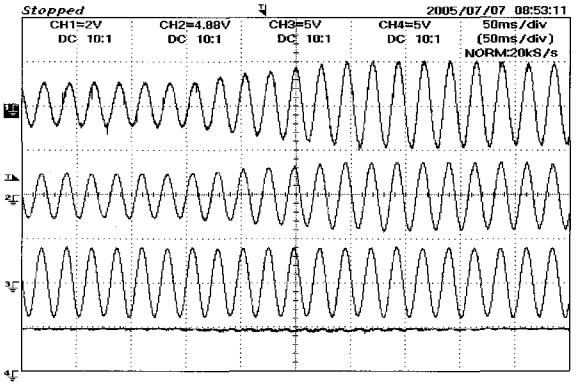

(1) Converter AC-side current -5A/div (2) IG current -5A/div
(3) IG voltage -250V/div (4) DC link voltage -250V/div

(b) in transient 43.1Hz-42.6Hz

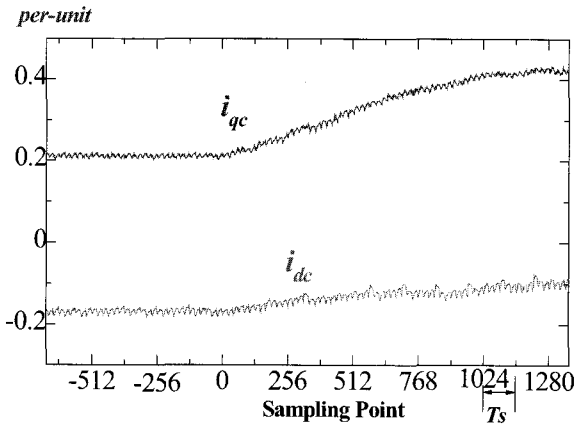

(d) *d-q* axis currents of PWM converter

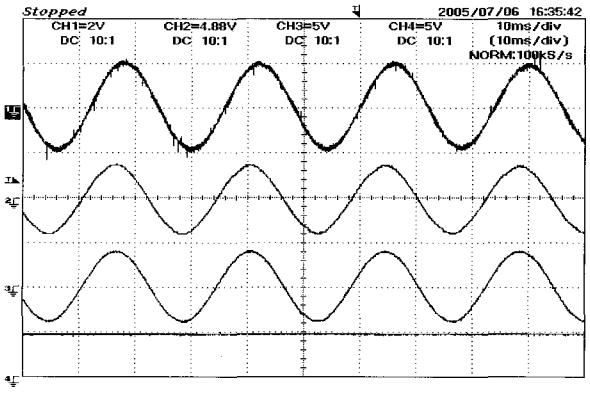

(1) Converter AC-side current -5A/div (2) IG current -5A/div
(3) IG voltage -250V/div (4) DC link voltage -250V/div

(c) after step change (42.6Hz)

Fig. 11 Measured operating waveforms of IG system at n = 1760 rpm

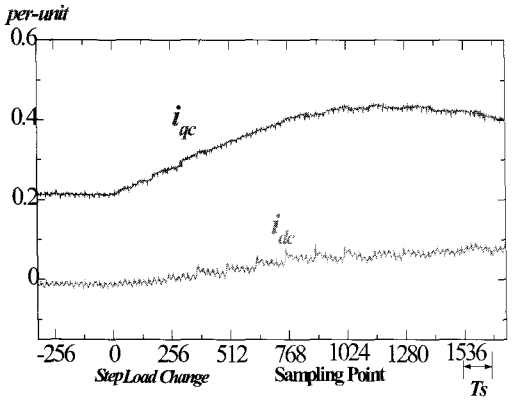

(d) *d-q* axis currents of PWM converter

Fig. 12 Measured operating waveforms of IG system at n = 1330 rpm

5. Voltage Regulation with AC Load

The size of the PWM converter as well as the system cost can be drastically reduced by disconnecting the DC load from the DC-link side of the PWM converter and connecting it through a diode rectifier for DC application[9]. For a three-phase load only, the PWM converter with the fixed excitation capacitor works to control the reactive power and requires a very small amount of active power to keep the DC-link voltage of the PWM converter constant. Several tests have been carried out to study the performance under both transient and steady-state conditions for AC load only. When resistive load is used as a heater, in actual applications especially, the frequency of the IG changes slightly. Fig.13 and Fig.14 indicate the measured waveforms of the AC load current, the AC-side current of the converter, the IG current and the IG line-to-line voltage for the case of a three-phase load power stepped from 16% to 50%, while the prime mover speed is kept constant at different speeds of 1550 rpm and 1300 rpm. In this case, the reactive component of the PWM converter is controlled to cancel the voltage drop caused by the step increasing of the active current, while the output frequency has been changed slightly from 49.8 Hz to 49.1 Hz at 1550 rpm and from 42.8 Hz to 41.9 Hz at1300 rpm. Based on these results, the proposed system proves that it can regulate the line-to-line voltage of the IG over a wide speed range.

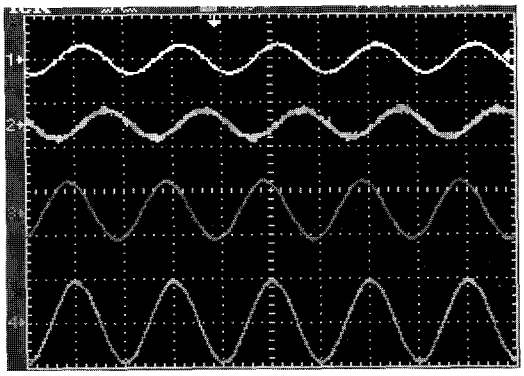

(1) AC load current -5A/div (2) Converter current -5A/div
(3) IG current – 5 A/div (4) IG voltage -250V/div at n = 1300rpm

(a) before step change 49.8Hz

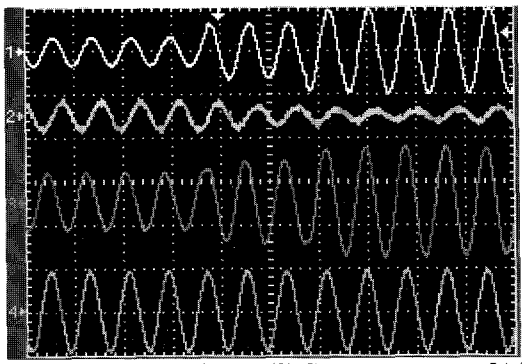

(1) AC load current -5A/div (2) Converter current -5A/div
(3) IG current – 5 A/div (4) IG voltage -250V/div at n = 1300rpm

(b) in transient 49.8Hz to 49.1 Hz

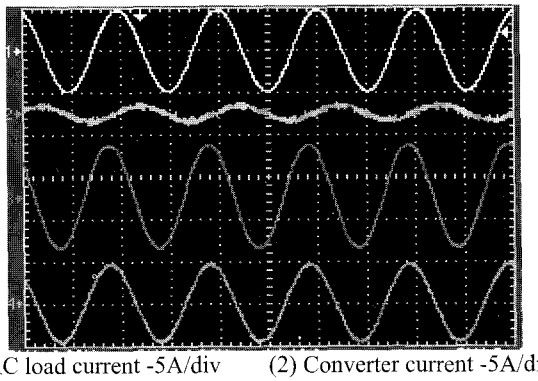

(1) AC load current -5A/div (2) Converter current -5A/div
(3) IG current – 5 A/div (4) IG voltage -250V/div at n = 1300rpm

(c)after step change 49.1 Hz

Fig. 13 Measured waveforms of the IG system with AC load power stepped from 16% to 50% of full-load power and speed(n = 1543rpm)

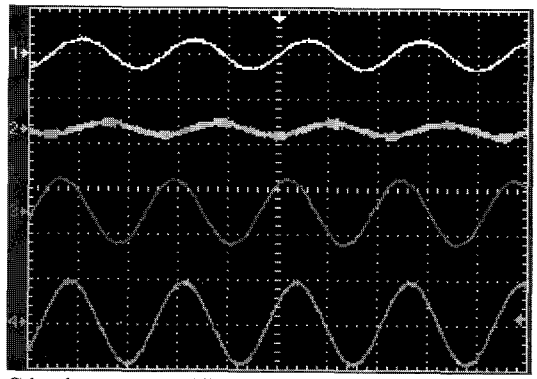

(1) AC load current -5A/div (2) Converter current -5A/div
(3) IG current – 5 A/div (4) IG voltage -250V/div at n = 1300rpm

(a) before step change 42.9Hz

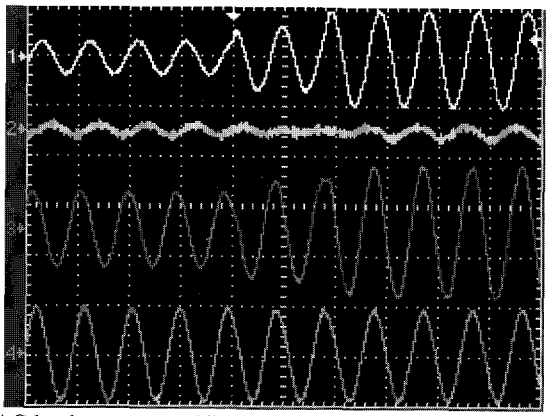

(1) AC load current -5A/div (2) Converter current -5A/div
(3) IG current – 5 A/div (4) IG voltage -250V/div at n = 1300rpm

(b) in transient 42.9Hz to 41.9 Hz

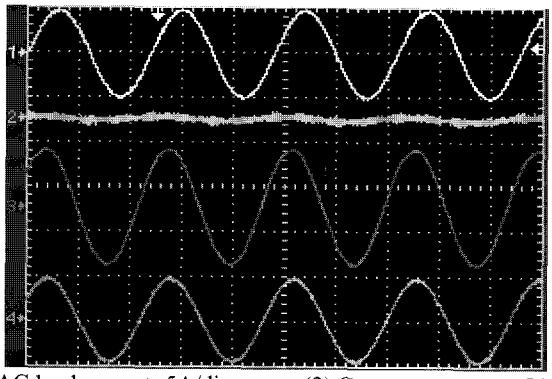

(1) AC load current -5A/div (2) Converter current -5A/div
(3) IG current – 5 A/div (4) IG voltage -250V/div at n = 1300rpm

(c) after step change 41.9 Hz

Fig. 14 Measured waveforms of IG system with AC load power stepped from 16% to 50% of full-load power and speed (n = 1300 pm)

6. IG Terminal Voltage Estimation by Deadbeat Controller

Fig.15 shows the transient responses of the d-q axis components of the stator voltage space vector v_s under the same conditions of the DC load step change from 16% to 50%. The proposed designed integrator as described in (16) gives considerably higher estimation accuracy while also eliminating the measuring errors.

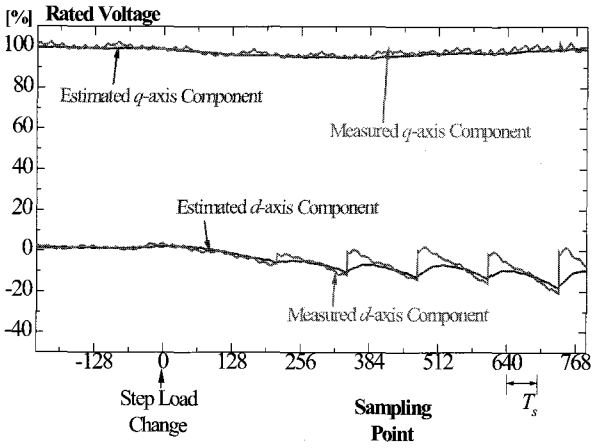

Fig. 15 IG terminal voltage estimation by deadbeat controller

7. IG Voltage Regulation with Speed Variation

Fig.16 shows a summary of all the measurements with the change in speed of the prime mover. The AC voltage regulation can be achieved over a wide range of speeds using the PI controller which adjusts the converter reactive current appropriately. The per-phase reactive current of the capacitor bank depends on the output frequency of the IG. Therefore, any voltage drop due to the active current has to be compensated for by the PWM converter reactive current. For a wider operating speed range, a smaller converter size can be used. For example, if the speed range is between 0.7 per unit and 0.96 per unit at the half-full load operation, the maximum inverter current will be only 10% of the rated current of the IG.

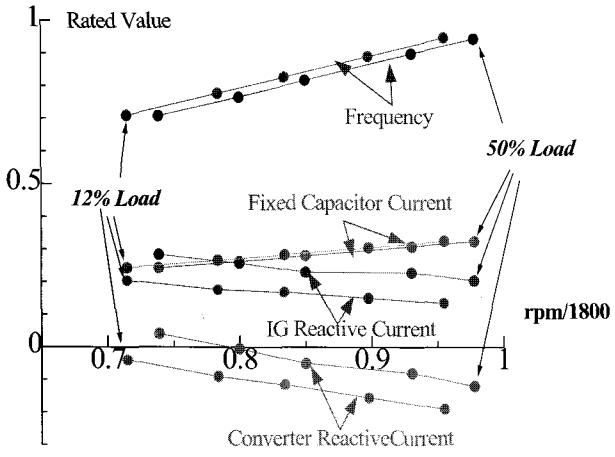

12% Load is for three-phase resistive load, 260W
50% Load is 260W three-phase resistive load and 800W DC Load

Fig. 16 Steady-state operating performance of the IG system and the hybrid excitation system (PWM converter and the capacitor bank) with speed variation

8. Conclusions

This paper has provided an advanced solution for wind turbine generators by applying an induction machine field oriented control. It then described a rotor field-oriented vector controlled induction generator for small-scale AC and DC power applications. The magnetization curve of the IG has been included in the proposed control system to more accurately calculate the rotor flux position in spite of the control complexity, which lies in the fact that stable grid voltages are not available. Matlab / Simulink environments supported the control for the IG excited by a capacitor bank and PWM converter for operating within a wide range of change in AC and DC loads. This proposed control system provided good voltage regulation for speeds less than 0.9 per unit where the IG could be advantageous in wind power applications.

Moreover, a deadbeat current controller was also proposed for a stand-alone IG scheme working with variable speed and supplying DC and three-phase loads with a voltage regulation scheme. The significant features of this controller are that it uses only three sensors for detecting the DC bus voltage of the PWM converter and the input currents of the PWM converter. The implementation of the controller neither needs a mechanical position nor a speed-sensing system. Therefore, the system is both highly reliable and exhibits low cost.

References

[1] T. Ahmed, O. Noro, E. Hiraki and M. Nakaoka, "Terminal Voltage Regulation Characteristics by Static VAR Compensator for a Three-Phase Self-Excited Induction Generator", IEEE Transactions on Industry Applications, Vol.40, No.4, pp.978–988, July-August 2004.

[2] E. Suarez and G. Bortolotto, "Voltage-Frequency Control of A Self-Excited Induction generator", IEEE Trans. on Energy Conversion, Vol.14, No.3 pp.394-401, September, 1999.

[3] E. Muljadi and T. A. Lipo, "Series compensated PWM inverter with battery supply applied to an isolated induction generator," IEEE Trans. Ind. Applicat., vol. 30, pp. 1073–1082, July/Aug. 1994.

[4] E. G. Marra and J. A. Pomilio, "Self-excited induction generator controlled by a VS-PWM bidirectional converter for rural applications," IEEE Trans. Ind. Applicat., vol. 35, pp. 877–883, July/Aug. 1999.

[5] O. Ojo and I. Davidson, "PWM-VSI inverter assisted stand-alone dual stator winding induction generator," in Conf. Rec. IEEE-IAS Annu. Meeting, Oct. 1999, pp. 1573–1580.

[6] D. Seyoum, F. Rahman, C. Grantham, "Terminal Voltage Control of a Wind Turbine Driven Isolated Induction Generator Using Stator Orientated Field Control", IEEE APEC Conf. Rec., Miami Beach, Vol. 2, pp 846-852, 2003.

[7] M. Naidu and J. Walters, "A 4-kW 42-V Induction-Machine-Based Automotive Power Generation System With a Diode Bridge Rectifier and a PWM Inverter", IEEE Trans. on Industry Applications, Vol.39, No.5 pp.1287-1293, September/October, 2003.

[8] R. Leidhold, G. Garcia and M.I. Valla, "Induction generator Controller Based on the Instantaneous Reactive Power Theory", IEEE Trans. on Energy Conversion, Vol.17, No.3 pp.368-373, September, 2002.

[9] T. Ahmed, K. Nishida and M. Nakaoka, "A Novel Induction Generator System for Small-Scale AC and DC Power Applications", Proceedings of the 36th Annual Power

Electronics Specialists Conference, IEEE- PESC 05, Vol.1, pp.250 –256, 12-16 June 2005.

Tarek Ahmed received his Ph.D. in Electrical Engineering from the Graduate School of Science and Engineering, Yamaguchi University, Yamaguchi, Japan in 2006. He is working as an Associate Professor in the Electrical Engineering Department, Faculty of Engineering, Assiut University, Assiut, Egypt. He is currently a Postdoctoral Fellow of the Japan Society for the Promotion of Science (JSPS) in the Power Electronic System and Control Engineering Laboratory, the Division of Electrical and Electronic Systems Engineering, Yamaguchi University, Yamaguchi, Japan. His research interests are in the design and control of PWM rectifier and sinewave PWM inverter power conditioners for renewable energy power generation systems. He has received the Paper Awards from the Institute of Electrical Engineers of Japan in 2003, in 2004, and in 2004, the best student award from IEEE-IECON'04 and best paper award from IEEE-ICEMS'04. Dr. Ahmed is a member of the Institute of Electrical and Electronics Engineers of USA.

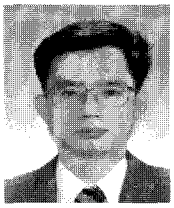

Katsumi Nishida received his B.Sc., and M.Sc. degrees in electrical engineering from the Tokyo Institute of Technology, Tokyo in 1976 and 1978, respectively. He received his Ph.D. from the Division of Electrical and Electronic Systems Engineering at the Graduate School of Science and Engineering, Yamaguchi University, Yamaguchi, Japan in 2002. He is currently working as a Professor in the Department of Electrical Engineering, Ube National College of Technology, Yamaguchi, Japan. He is engaged in research on power factor correction of PWM converters and current control of the three-phase active power filters using the dead-beat and the adaptive signal processing technique. Dr. Nishida is a member of the Institute of Electrical and Electronics Engineers of the USA (IEEE-USA), the Institute of Electrical Engineers of Japan (IEE-Japan) and the Japan Institute of Power Electronics (JIPE).

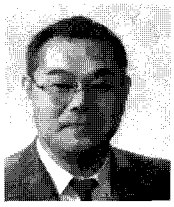

Mutsuo Nakaoka received his Ph.D. in Electrical Engineering from Osaka University, Osaka, Japan in 1981. He joined the Electrical and Electronics Engineering Department, Kobe University, Kobe, Japan in 1981. Since 1995, he has worked as a professor in the Electrical and Electronics Engineering Department, the Graduate School of Science and Engineering and Science, Yamaguchi University, Yamaguchi, Japan. Now he is an Emeritus professor. His research interests include state-of-the-art power electronics circuits and systems engineering. Dr. Nakaoka is a member of the Institute of Electrical Engineers of Japan, the Institute of Electronics, Information, and Communication Engineers of Japan, the Institute of Illumination Engineering of Japan, the Power Electronics Society of Japan, the Institute of Installation Engineers of Japan and a Senior Member of IEEE, USA

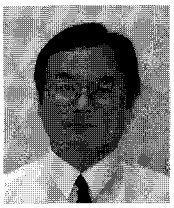

Toshihiko Tanaka received the M.S. degree from Nagaoka University of Technology in 1984. In 1995, he received his Ph.D. from Okayama University. He joined Toyo Denki Mfg. Co. in 1984. From 1991 to 1997, he was an Assistant Professor at the Polytechnic University of Japan. From 1997 to 2004 he was an Associate Professor at Shimane University. Since 2004, he has been a Professor in the Department of Electrical and Electronic Engineering at Yamaguchi University. His research interests are in harmonics generated by static power converters and their compensation. Dr. Tanaka is a member of the Institute of Electrical and Electronic Engineers and the Institute of Electrical Engineers of Japan.